



# Black Hole Hyperaccretion in Collapsars. II. Gravitational Waves

Yun-Feng Wei and Tong Liu

Department of Astronomy, Xiamen University, Xiamen, Fujian 361005, People's Republic of China; [tongliu@xmu.edu.cn](mailto:tongliu@xmu.edu.cn)*Received 2019 September 27; revised 2019 December 6; accepted 2019 December 16; published 2020 January 28*

## Abstract

As progenitors of gamma-ray bursts (GRBs), the core collapse of massive stars and the coalescence of compact object binaries are believed to be powerful sources of gravitational waves (GWs). In the collapsar scenario, a rotating stellar-mass black hole (BH) surrounded by a hyperaccretion disk might be active in the center of a massive collapsar, which is one of the plausible central engines of long GRBs. Such a BH hyperaccretion disk would be in a state of a neutrino-dominated accretion flow (NDAF) at the initial stage of the accretion process; meanwhile, the jets attempt to break out from the envelope and circumstellar medium to power GRBs. In addition to collapsars, BH hyperaccretion systems are important sources of neutrinos and GWs. In this paper, we investigate the GW emission generated by the anisotropic neutrino emission from NDAFs in collapsar scenarios. As the results indicate, the typical frequency of GWs is  $\sim 1\text{--}100$  Hz, and the masses and metallicities of the progenitor stars have slight effects on the GW strains. The GWs from NDAFs might be detected by operational or planned detectors at a distance of 10 kpc. Moreover, comparisons of the detectable GWs from collapsars, NDAFs, and GRB jets (internal shocks) are displayed. By combining the electromagnetic counterparts, neutrinos, and GWs, one may constrain the characteristics of collapsars and central BH accretion systems.

*Unified Astronomy Thesaurus concepts:* [Accretion \(14\)](#); [Stellar mass black holes \(1611\)](#); [Neutrino astronomy \(1100\)](#); [Core-collapse supernovae \(304\)](#); [Gravitational waves \(678\)](#); [Gamma-ray bursts \(629\)](#); [Relativistic jets \(1390\)](#)

## 1. Introduction

The detection of gravitational waves (GWs) from the binary black hole (BH) merger GW150914 by the Laser Interferometer Gravitational-Wave Observatory (LIGO) marks that we have entered an era of GW astronomy (Abbott et al. 2016). The detection of a GW event from a binary neutron star (NS) merger system GW170817 (Abbott et al. 2017) that was associated with electromagnetic signals marked the beginning of multimessenger astronomy with GWs. In the future, astrophysical sources including massive star collapse, rapidly rotating NSs, and other violent events in the universe might be detected by GW detectors (e.g., Cutler & Thorne 2002). Such events are promising multimessenger transient sources, especially for massive star collapse.

Observational evidence has indicated that core-collapse massive stars are the progenitors of long-duration gamma-ray bursts (LGRBs; see the review by Woosley & Bloom 2006; Kumar & Zhang 2015). The majority of LGRB host galaxies are irregular, star-forming galaxies (e.g., Fruchter et al. 2006). A handful of LGRBs are associated with core-collapse supernovae (CCSNe, see, e.g., Galama et al. 1998; Hjorth et al. 2003; Stanek et al. 2003; Malesani et al. 2004; Modjaz et al. 2006; Pian et al. 2006). Note that CCSNe are diverse, broadly partitioned in normal (narrow line) and relatively more energetic (broad line) events (e.g., Maurer et al. 2010; van Putten et al. 2011). The observations show that some broad-lined and bright type Ib/c SNe are accompanied by LGRBs. In the collapsar model (e.g., Woosley 1993; MacFadyen & Woosley 1999; Woosley et al. 2002; Zhang et al. 2004; Woosley & Heger 2012), the core of the massive star will collapse; then a few  $M_{\odot}$  BH surrounded by a temporary disk with a very high accretion rate might be formed. As a plausible central engine of LGRBs, this accretion process can launch powerful jets. If the activity of the central engine lasts long

enough to allow the jets to break out from the envelope and circumstellar medium (CSM), an energetic LGRB will be triggered.

Generally, a BH hyperaccretion system can launch gamma-ray burst (GRB) jets via two well-known mechanisms: the neutrino–antineutrino annihilation process, and the Blandford–Znajek (BZ, Blandford & Znajek 1977) mechanism. If the accretion rate is very high ( $\sim 0.001\text{--}10 M_{\odot} \text{s}^{-1}$ ), then the photons are trapped in the disk, and generous neutrinos are produced. Neutrino pairs are emitted from the disk surface and annihilate above the disk to power GRBs. Such an accretion disk is called a neutrino-dominated accretion flow (NDAF), whose properties have been widely investigated in recent decades (e.g., Popham et al. 1999; Narayan et al. 2001; Kohri & Mineshige 2002; Lee et al. 2005; Gu et al. 2006; Chen & Beloborodov 2007; Janiuk et al. 2007; Kawanaka & Mineshige 2007; Liu et al. 2007, 2015, 2017a; Lei et al. 2009; Xue et al. 2013; Song et al. 2016; Nagataki 2018). In the BZ mechanism, the magnetic lines tied on the disk will fall into the BH, followed by the accretion materials; then, Poynting jets would be launched via extraction of the spin energy of the BH to power GRBs (e.g., Lee et al. 2000a, 2000b; McKinney & Gammie 2004; Mizuno et al. 2004; Barkov & Komissarov 2008; Nagataki 2009; Lei et al. 2013, 2017; Wu et al. 2013).

Nevertheless, for the very rapidly rotating BHs surrounded by magnetized disks or toruses, the temporal evolution of the accretion onto the BHs may subject to large-scale magnetic torques (van Putten & Ostriker 2001). Thus the accretion mode will be changed. The additional spin-up torque from the BH may arrest the inflow for the duration of the BH spin-down lifetime. Therefore, the activity duration of the central engine can be derived from both the timescale of accretion flow and the lifetime of the BH spin, which are also well known in the active galactic nuclei community (O’Dea 2002). van Putten (2001) suggested that LGRBs arise with rapidly spinning BHs

in the suspended accretion, while short GRBs arise with slowly spinning BHs.

Multimessenger observations are essential to constrain the characteristics of collapsars, especially for the central BH accretion systems. It is difficult to extract the information of the central engine from electromagnetic signals, as the most observed electromagnetic signals from GRBs are produced in the regions far from the central engines (Cutler & Thorne 2002). Neutrinos and GWs can provide us with the information hidden deep inside the stellar cores. The detectable MeV neutrinos from NDAFs have been discussed in Liu et al. (2016). These neutrinos can reach a luminosity of  $10^{50}$ – $10^{51}$  erg s<sup>-1</sup>, peaking at  $\sim 10$  MeV, and might be observed by the next generation MeV neutrino detectors, such as Hyper-Kamiokande, when the events are close enough to Earth. GW emission from GRB central engines has been investigated in many previous works. Sun et al. (2012) studied the GWs from jet precession driven by an NDAF around a spinning BH. GWs generated by the anisotropic neutrino emission from NDAFs have been discussed in some studies (e.g., Suwa & Murase 2009; Liu et al. 2017b). Liu et al. (2017b) calculated the dependence of the GW strains from NDAFs on both the BH spin and accretion rate. They demonstrated that GWs from NDAFs might be detected at a distance of  $\sim 100$  kpc/ $\sim 1$  Mpc by the advanced LIGO/Einstein Telescope with a typical frequency of  $\sim 10$ – $100$  Hz. They made a comparison of GWs from different central engines of GRBs: NDAFs, BZ mechanisms (no GW emission), and millisecond magnetars. GWs from the central engines of adjacent GRBs might be used to determine whether there is an NDAF, BZ jets, or a magnetar. Furthermore, van Putten & Levinson (2003) studied the GWs from a magnetized torus around a rapidly rotating BH. They pointed out that the configuration of the accretion torus itself might develop to the large nonaxisymmetries. The torus converts  $\sim 10\%$  of the BH spin energy into gravitational radiation through a finite number of multipole mass moments and, to a lesser degree, into MeV neutrinos and winds. As demonstrated in van Putten et al. (2019), they estimated the total GW energy  $E_{\text{GW}} \simeq (3.5 \pm 1)\% M_{\odot} c^2$  from BH spin-down after post-merger in GW170817. GWs from the suspended accretion are expected to be detected by LIGO–Virgo up to the distances of about 100 Mpc (e.g., van Putten et al. 2019).

This paper is the second work in a series on BH hyperaccretion in collapsars. In Wei et al. (2019, hereafter Paper I), we investigated the MeV neutrino emission from NDAFs in collapsar scenarios. In the initial hundreds of seconds of the accretion process, the mass supply rate of the massive progenitor is generally higher than the ignition rate of NDAFs, but the jets are generally choked in the envelope. Thus, only neutrinos can be emitted from the center of a collapsar. We studied the effects of the masses and metallicities of the progenitor stars on the time-integrated spectra of electron neutrinos from NDAFs. The masses of collapsars have little influence on the neutrino spectrum, and the low metallicities are beneficial for the production of low-energy ( $\lesssim 1$  MeV) neutrinos. We also studied the differences in the electron neutrino spectra between NDAFs and proto-NSs (PNSs), which may help one to verify the possible remnants of the core collapse of massive stars with future neutrino detectors.

In this paper, we focus on the GW emission from NDAFs in collapsar scenarios and study the effects of the masses and

metallicities of the progenitor stars on the GW emission from NDAFs. Meanwhile, a comparison of GW signals from NDAFs, jets, and collapsars is displayed. The paper is organized as follows. In Section 2, we describe the progenitor model and show the method to calculate the GWs emitted by anisotropic neutrino emission. Based on the time evolution of the mass accretion of progenitors with different masses and metallicities, the GW emission of NDAFs in collapsar scenarios is studied. In addition, the detection of GW signals is discussed. In Section 3, we compare the GW emission from different phases of collapsars. A summary is presented in Section 4.

## 2. GWs from NDAFs in Collapsars

### 2.1. Progenitor Model

We adopt the presupernova (pre-SN) model (see, e.g., Woosley et al. 2002; Woosley & Heger 2007; Heger & Woosley 2010) in this work. After a massive star collapses, a rotating stellar-mass BH surrounded by a hyperaccretion disk might form. Using the density profiles of the pre-SN model (for details, see Paper I), we can calculate the mass supply rate of the progenitors (see, e.g., Suwa & Ioka 2011; Woosley & Heger 2012; Matsumoto et al. 2015; Liu et al. 2018, 2019), i.e.,

$$\dot{M}_{\text{pro}} = \frac{dM_r}{dt_{\text{ff}}} = \frac{dM_r/dr}{dt_{\text{ff}}/dr} = \frac{2M_r}{t_{\text{ff}}} \left( \frac{\rho}{\bar{\rho} - \rho} \right), \quad (1)$$

where  $M_r$  is the mass coordinate,  $\rho$  is the mass density of the progenitor star, and  $\bar{\rho} = 3M_r/(4\pi r^3)$  is the mean density within  $r$ . Here, we roughly set the accretion rate  $\dot{M}$  equal to the mass supply rate (e.g., Kashiyama et al. 2013; Nakauchi et al. 2013). The accretion timescale of each mass shell at radius  $r$  is roughly equal to the freefall timescale:

$$t_{\text{ff}} = \sqrt{\frac{3\pi}{32G\bar{\rho}}} = \frac{\pi}{2} \sqrt{\frac{r^3}{2GM_r}}. \quad (2)$$

In the collapsar scenarios, the duration of the central engine can be related to the fallback accretion of a progenitor envelope. For the suspended accretion (van Putten & Ostriker 2001), the activity duration of the central engine is expected to depend on the lifetime of the BH spin. Such a case is not considered in this work. In the initial hundreds of seconds of the accretion process, the jets are generally choked in the envelope of a collapsar, so no electromagnetic counterparts of the central engine can be observed (see, e.g., Kashiyama et al. 2013; Nakauchi et al. 2013; Liu et al. 2018, 2019; Song & Liu 2019). Whether the jets can break out depends on the activity timescale of the central engine, the scale and density of the dense CSM and the properties of the jets. If the activity of the central engine lasts long enough to allow the jets to break out of the envelope and CSM, an energetic LGRB will be triggered (e.g., Liu et al. 2018, 2019).

### 2.2. GWs from NDAFs

For NDAFs, there are some characteristic radii (e.g., Chen & Beloborodov 2007; Zalamea & Beloborodov 2011; Liu et al. 2017a, 2018; Zhang 2018), such as the ignition radius  $r_{\text{ign}}$ , which can be defined as the radius such that  $Q_{\nu}^-/Q_{\text{vis}} = 1/2$ , where  $Q_{\nu}^-$  and  $Q_{\text{vis}}$  are the neutrino cooling rate and the viscous

heating rate, respectively (e.g., Chen & Beloborodov 2007; Liu et al. 2017a). Inside the region of  $\lesssim r_{\text{ign}}$ , one can say that neutrino cooling processes are dominant. Therefore, an NDAF is ignited only when  $r_{\text{ign}}$  is larger than the inner radius of the disk. The corresponding mass accretion rate is  $\dot{M}_{\text{ign}}$ , which is mainly related to the BH spin and the viscous parameter of the disk. If  $\dot{M} < \dot{M}_{\text{ign}} \sim 0.001 M_{\odot} \text{ s}^{-1}$ , the neutrino emission can be ignored, and the disk is no longer called an NDAF. In the collapsar scenarios, the mass accretion onto the BH decreases over time, and the typical duration of the NDAF in the collapsar is hundreds of seconds.

Xue et al. (2013) investigated one-dimensional global solutions of NDAFs in the Kerr metric, taking into account the detailed neutrino physics, chemical potential equilibrium, neutrino trapping and nucleosynthesis. They calculated 16 solutions with different characterized accretion rates and BH spins. Based on the results, they fitted time-independent analytical formulas, and the neutrino luminosity  $L_{\nu}$  is given by

$$\log L_{\nu}(\text{erg s}^{-1}) \approx 52.5 + 1.17a_* + 1.17 \log \dot{m}, \quad (3)$$

where  $a_*$  ( $0 < a_* < 1$ ) is the mean dimensionless BH spin parameter, and  $\dot{m} = \dot{M}/M_{\odot} \text{ s}^{-1}$  is the dimensionless accretion rate. We adopt  $a_* = 0.9$  in our calculations.

According to the above formulas, we can roughly obtain the time evolution of the neutrino luminosity  $L_{\nu}(t)$ . The GW emission from NDAFs depends on the neutrino luminosity, and the typical GW frequency is related to the variabilities and duration of neutrino emission.

The GWs from anisotropic neutrino radiation were first analyzed by Epstein (1978). We adopt the methods applied to CCSNe (e.g., Burrows & Hayes 1996; Müller & Janka 1997; Kotake et al. 2006, 2007) to calculate the GWs from NDAFs in the collapsar scenarios.

With the angles  $\theta'$  and  $\phi'$  defining the radiation direction in the source coordinate frame, the GW amplitude is given by (e.g., Müller & Janka 1997; Suwa & Murase 2009)

$$h_{+}(t, \vartheta) = \frac{2G}{Rc^4} \int_{-\infty}^{t-R/c} dt' \int_{4\pi} d\Omega' \Psi(\theta', \phi', \vartheta) \times \frac{dL_{\nu}(\theta', t')}{d\Omega'}, \quad (4)$$

where  $\vartheta$  is the viewing angle,  $R$  is the distance from the observer to the source,  $dL_{\nu}/d\Omega'$  represents the direction-dependent neutrino luminosity per unit of solid angle in the direction of  $\Omega'$ , and  $\Psi(\theta', \phi', \vartheta)$  denotes the angle dependent factor,

$$\Psi(\theta', \phi', \vartheta) = (1 + \cos \theta' \cos \vartheta + \sin \theta' \cos \phi' \sin \vartheta) \times \frac{(\sin \theta' \cos \phi' \cos \vartheta - \cos \theta' \sin \vartheta)^2 - \sin^2 \theta' \sin^2 \phi'}{(\sin \theta' \cos \phi' \cos \vartheta - \cos \theta' \sin \vartheta)^2 + \sin^2 \theta' \sin^2 \phi'}. \quad (5)$$

When  $dL_{\nu}/d\Omega'$  is axisymmetric, the counterpart of the amplitude,  $h_{\times}^{TT}$ , vanishes (for details, see Suwa & Murase 2009). In this work, we suppose the NDAF is a geometrically infinitely thin disk and assume that the emission of neutrinos is isotropic at any point of the disk surface. The neutrino luminosity per solid angle can be written as  $dL_{\nu}/d\theta' = L_{\nu} |\cos \theta'|/2\pi$ . Then,

Equation (4) is integrated analytically as

$$h_{+}(t, \vartheta) = \frac{1 + 2 \cos \vartheta}{3} \tan^2 \left( \frac{\vartheta}{2} \right) \frac{2G}{Rc^4} \times \int_{-\infty}^{t-R/c} L_{\nu}(t') dt'. \quad (6)$$

Here, we can see the dependence of the GW amplitude on the viewing angle  $\vartheta$ . For  $\vartheta = \pi/2$ , the observer is located in the equatorial plane of the disk, and the GW amplitude is the largest.

The local energy flux of GWs is given by (e.g., Suwa & Murase 2009; Liu et al. 2017b)

$$\frac{dE_{\text{GW}}}{R^2 d\Omega dt} = \frac{c^3}{16\pi G} \left| \frac{d}{dt} h_{+}(t, \vartheta) \right|^2, \quad (7)$$

where  $\Omega$  is the solid angle in the observer coordinate frame.

The total GW energy can be obtained by

$$E_{\text{GW}} = \frac{\beta G}{9c^5} \int_{-\infty}^{\infty} dt L_{\nu}(t)^2, \quad (8)$$

where  $\beta \sim 0.47039$ .

To obtain a GW spectrum,  $L_{\nu}(t)$  is written in terms of the inverse Fourier transform as

$$L_{\nu}(t) = \int_{-\infty}^{+\infty} \tilde{L}_{\nu}(f) e^{-2\pi i f t} df; \quad (9)$$

then, one can deduce the GW energy spectrum as

$$\frac{dE_{\text{GW}}(f)}{df} = \frac{2\beta G}{9c^5} |\tilde{L}_{\nu}(f)|^2. \quad (10)$$

To estimate the detectability of the GWs, the characteristic GW strains are defined by

$$h_c(f) = \frac{1}{R} \sqrt{\frac{2}{\pi^2} \frac{G}{c^2} \frac{dE_{\text{GW}}(f)}{df}} \quad (11)$$

for a given frequency  $f$  (Flanagan & Hughes 1998). Since we obtain the characteristic GW strains, the signal-to-noise ratios (S/Ns) obtained from the matched filtering for the GW detectors can be calculated. The S/N for an optimally oriented source is

$$S/N^2 = \int_0^{\infty} d(\ln f) \frac{h_c(f)^2}{h_n(f)^2}, \quad (12)$$

where  $h_n f = \sqrt{5f S_h(f)}$  is the noise amplitude and  $S_h(f)$  is the spectral density of the strain noise in the detector at frequency  $f$ .

### 2.3. Results

We selected progenitor metallicities of  $Z/Z_{\odot} = 1, 0.1, 0.01$ , and  $10^{-4}$  and masses of  $M_{\text{pro}}/M_{\odot} = 20, 30, 40$ , and  $60$ , where  $Z_{\odot}$  is the metallicity of the Sun, to investigate the effects of the mass and metallicity on the GW emission of NDAFs. Based on the density profiles of the progenitor stars with different masses and metallicities (for details, see Paper I), we can calculate the time evolution of the mass accretion rate of progenitor stars, as shown in Figure 1. The blue, red, green, and black curves correspond to progenitor masses of  $M_{\text{pro}}/M_{\odot} = 20, 30, 40$ , and  $60$ , respectively. The different density profiles of the progenitor stars cause the difference in  $\dot{M}$ . In the initial accretion stage, the mass accretion rates are all approximately  $1 M_{\odot} \text{ s}^{-1}$ , which are

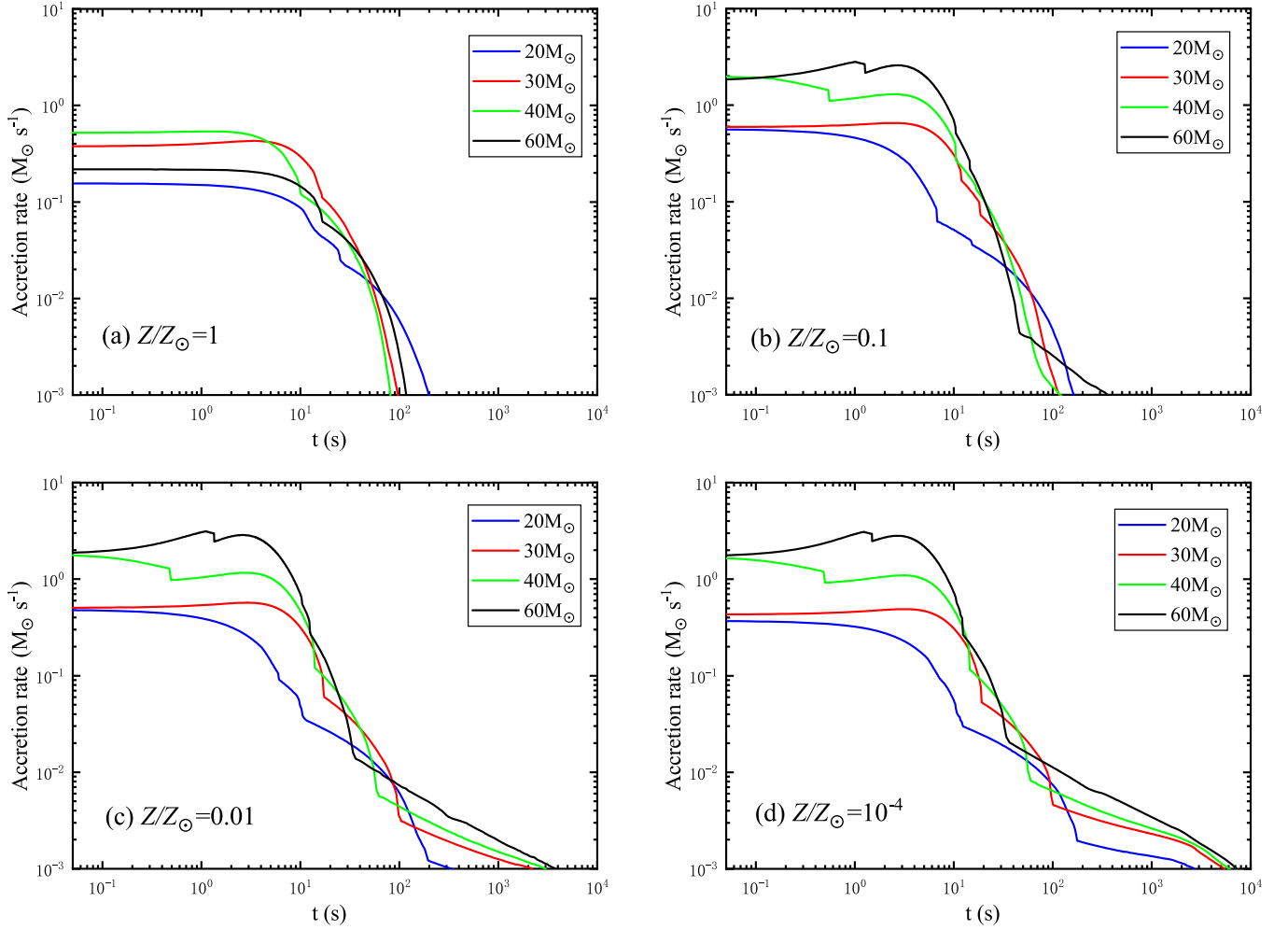


**Figure 1.** Time evolution of the mass accretion rate (mass supply rate) of progenitor stars with different masses  $M_{\text{pro}}$  and metallicities  $Z$ . The blue, red, green, and black curves correspond to progenitor masses of  $M_{\text{pro}}/M_{\odot} = 20, 30, 40,$  and  $60$ , respectively.

typical mass accretion rates of NDAFs. The metallicities can affect the duration of the neutrino emission in collapsars, while the progenitor mass plays an important role in the time evolution of the mass accretion rate.

Figure 2 shows the strains of the GWs from NDAFs in the center of collapsars at a distance of 10 kpc. The blue, red, green, and black curves correspond to the progenitor masses of  $M_{\text{pro}}/M_{\odot} = 20, 30, 40,$  and  $60$ , respectively. Sensitivity lines (the noise amplitudes  $h_n$ ) of Advanced LIGO (aLIGO), the Einstein Telescope (ET), *LISA*, the *Decihertz Interferometer Gravitational Wave Observatory/Big Bang Observer (DECIGO/BBO)*, and *ultimate-DECIGO* are shown in these figures. As the progenitor mass increases, the mass accretion rate onto the BH tends to slightly rise in the initial accretion phase, as shown in Figure 1, so the GW strains increase within an order of magnitude. Meanwhile, the progenitor metallicities also have little influence on the GW strains, as the accretion rates in the initial accretion stage show little difference for the different metallicities and the same mass. Although the lower metallicities correspond to a longer duration of neutrino emission, the neutrino cooling is invalid in the late accretion stage. Overall, the GW signals from NDAFs in the center of the massive progenitor stars are more likely to be detected at the distance of 10 kpc.

The effects of the distance on the detection of GW signals from NDAFs are clearly displayed in Figure 3. At a distance

of  $\sim 10$  kpc, the GWs from NDAFs in the center of the very massive progenitors might be detected by *DECIGO/BBO* and *ultimate-DECIGO* and by ET and aLIGO in the detectable frequency range of  $\sim 10$ – $100$  Hz. Even so, it is difficult to distinguish the characteristics of the progenitor stars from the GW detection, as shown in Figure 2. Multimessenger observations, including electromagnetic and neutrino emissions, are indispensable for constraining the nature of the progenitor stars, as well as that of the central BH hyperaccretion systems. Moreover, one can see that the GW signals of NDAFs at the distance of 1 Mpc are almost impossible to detect by the operational or planned detectors.

Note that the star rotation was neglected in the above pre-SN model. For the moderately rotating stars, the rotation has limited effects on the neutrino emission from NDAFs. However, as shown in Janiuk & Proga (2008), the various rotation profiles imposed on the collapsing stars may significantly change the evolution of GRBs. Thus, for fast-rotating progenitor stars, the rotation might significantly change the GW signals from NDAFs.

### 3. GW Emission in Massive Collapsars

GW emission from collapsars has been investigated for approximately four decades. Numerous numerical simulations predicted that GWs from various phenomena associated with gravitational collapse could be detected by ground-based and

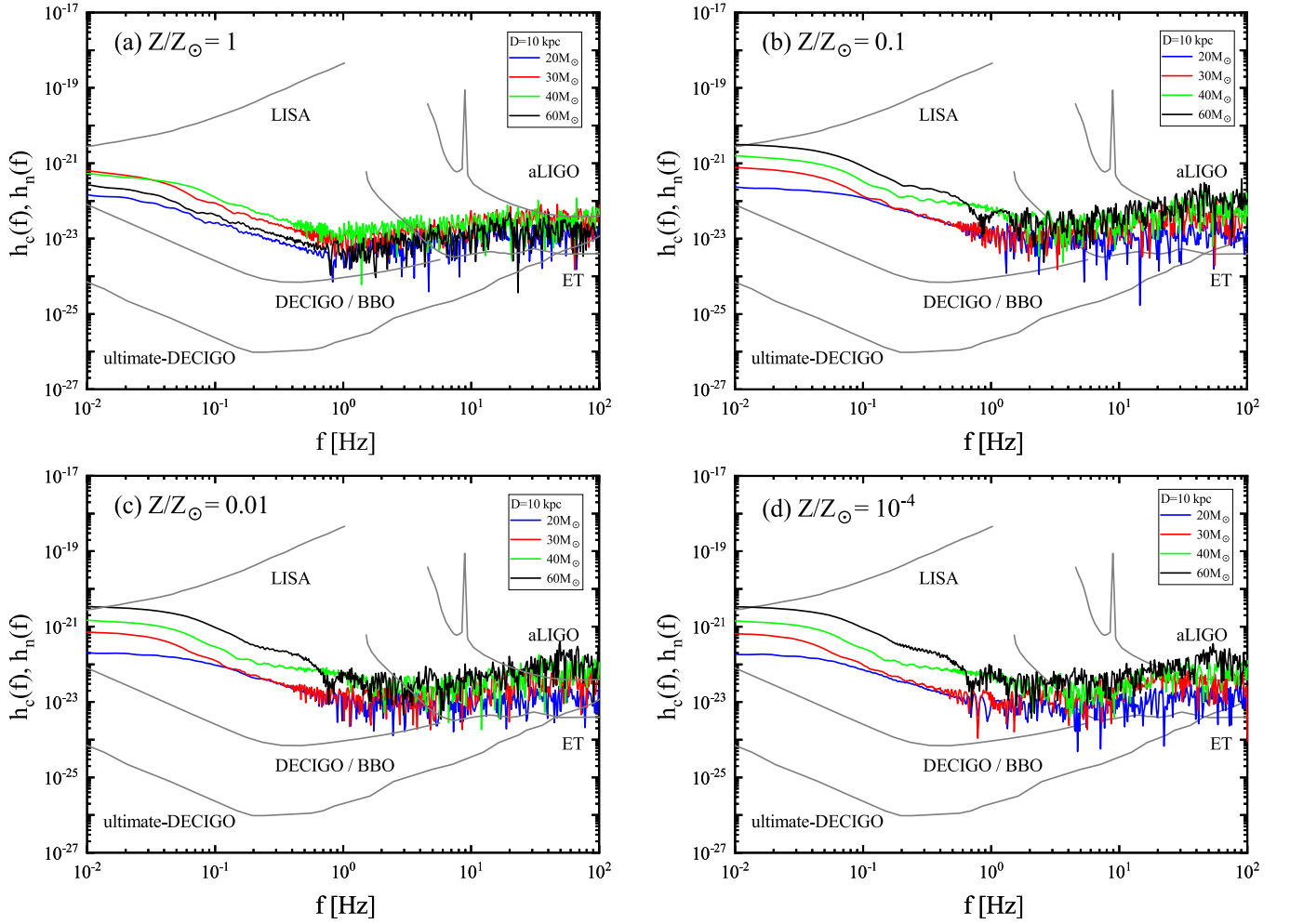


**Figure 2.** The strains of the GWs from NDAFs in the center of collapsars at the distance of 10 kpc. The blue, red, green, and black curves correspond to progenitor masses of  $M_{\text{pro}}/M_{\odot} = 20, 30, 40,$  and  $60$ , respectively. In all four figures, the gray lines show the sensitivity lines (the noise amplitudes  $h_n$ ) of aLIGO, ET, LISA, DECIGO/BBO, and ultimate-DECIGO.

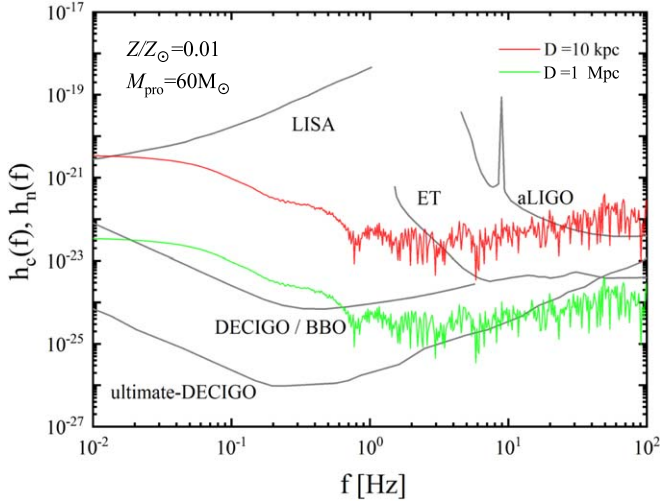


**Figure 3.** The dependence of the GW strains on the distances. The mass and metallicity of the progenitors are  $M_{\text{pro}}/M_{\odot} = 60$  and  $Z/Z_{\odot} = 0.01$ , respectively.

space-based interferometric GW detectors (see the review by Fryer & New 2011). For most of the massive stars, the GW signals from core collapsars will be similar to those from

normal CCSNe, whose GW signals have been widely investigated (see the review by Ott 2009; Kotake 2013). If the core collapsars and/or the resulting supernova (SN) explosions are nonspherical such that the third time derivative of the quadrupole moment of the mass–energy distribution is nonzero, part of the liberated gravitational binding energy will be emitted in the form of GWs. Such nonsphericities can be caused by the effects of rotation, convection and anisotropic neutrino emission. These effects lead either to small-scale statistical mass–energy fluctuations or large-scale asphericities (e.g., Epstein 1978; Müller 1982; Moenchmeyer et al. 1991; Herant 1995; Yamada & Sato 1995; Burrows & Hayes 1996; Müller & Janka 1997; Zwerger & Müller 1997; Rampp et al. 1998; Dimmelmeier et al. 2002; Fryer et al. 2002, 2004b; Müller et al. 2004; Ott et al. 2004). In the collapsar scenarios, a massive star will go through the collapse, bounce, and postbounce phase, then BH formation, the hyperaccretion phase, and the GRB jet phase (e.g., Ott et al. 2011; Kotake et al. 2012). From the perspective of detecting GWs, we divide this evolutionary process into three periods: the collapsar phase (from collapse and bounce to BH formation), central engine phase (hyperaccretion phase) and GRB jet phase. We study the typical frequencies and amplitudes of GW signals from these three different phases and plot the results in Figure 4. The blue, purple, and orange shaded regions represent

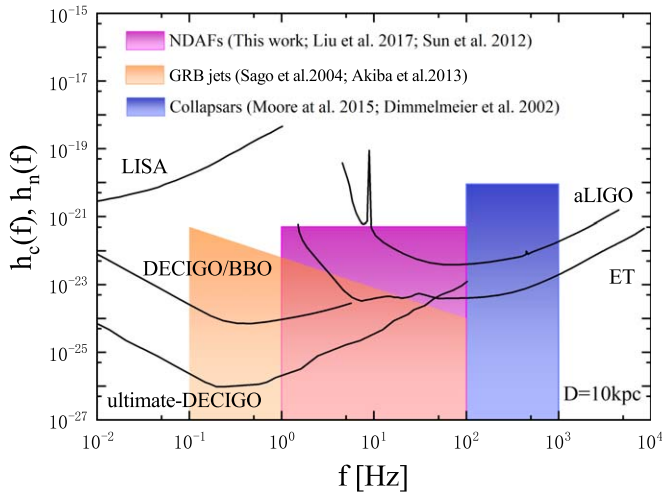


**Figure 4.** The characteristic amplitude of GWs from different sources in a collapsar. The blue, purple, and orange shaded boxes represent the collapsar phase, NDAFs, and GRB jet phase, respectively. The gray lines show the sensitivity lines (the noise amplitudes  $h_n$ ) of aLIGO, ET, LISA, DECIGO/BBO, and ultimate-DECIGO. The distance is 10 kpc.

the collapsar phase, NDAFs and GRB jet phase, respectively. The detection distance is 10 kpc. The characteristic amplitude of GWs from the suspended accretion is not included in Figure 4. The GWs from the nonaxisymmetric accretion flow around a rapidly rotating BH are expected to be detected up to distance of about 100 Mpc (van Putten et al. 2019). At the distance of 10 kpc, the characteristic amplitude of the GWs from the suspended accretion is much larger than that from NDAFs.

In the collapsar phase, the primary GW signals are unlikely to be different from normal CCSNe. Most of the original studies paid attention to the strong GW signals produced at the rotating collapse and core bounce phase due to the large-scale aspherical motion of matter. The peak amplitude is roughly proportional to the collapsar spin. The typical frequency is expected to be 100–1000 Hz (see e.g., Kotake et al. 2006; Ott 2009; Kotake 2013).

In the postbounce phase, the anisotropic matter motions associated with the convection, anisotropic neutrino radiation, and standing-accretion-shock instability (SASI, e.g., Blondin et al. 2003; Burrows et al. 2006; Blondin & Mezzacappa 2006; Foglizzo et al. 2007; Kotake et al. 2007; Scheck et al. 2008) are expected to be the primary sources for GWs. Convective instability is an important feature of the postbounce evolution of massive stars (see, e.g., Buras et al. 2006; Burrows et al. 2006, 2007; Janka et al. 2007; Janka & Müller 1996). The convective overturn is expected as the entropy- and lepton-gradient-driven prompt convection that may occur immediately after bounce, lepton-gradient driven PNS convection, and neutrino-driven convection in the postshock heating region (e.g., Burrows & Lattimer 1983; Fryer & Heger 2000; Ott et al. 2008). The SASI caused by either an advective acoustic or a purely acoustic feedback cycle would lead to the growth of perturbations in the stalled shock (e.g., Blondin et al. 2003; Blondin & Mezzacappa 2006; Foglizzo et al. 2007; Scheck et al. 2008). When the SASI enters a nonlinear phase, it would heavily distort the postshock region and affect convection. Both the convection and SASI would lead to time-varying mass-quadrupole moments giving rise to a long-duration stage

of large amplitude GW emission. A semiquantitative summary of the GW emission by the aspherical fluid motions associated with the convection and SASI is given by Ott (2009). Based on numerous previous simulations (e.g., Müller et al. 2004; Ott et al. 2006; Marek et al. 2009), they provided estimations for the typical GW strains at 10 kpc, with the typical emission frequency  $f$  approximately in the range of 100–1000 Hz.

For the core collapse of massive stars, anisotropic neutrino emission may arise (a) from the global asymmetries in the (pre)collapse matter distribution (see, e.g., Burrows & Hayes 1996; Fryer et al. 2004a), (b) from the convective overturn and SASI (see, e.g., Ott et al. 2006; Kotake et al. 2007; Marek et al. 2009), and (c) from the rotationally deformed PNSs (e.g., Müller et al. 2004; Kotake et al. 2006). In contrast to the rapidly varying GW waveforms from matter motion, the GW waveforms from the anisotropic neutrino emission show a long-timescale variability. Hence, the anisotropic neutrino emission dominates the GW spectrum at low frequencies (below  $\sim 100$  Hz) (e.g., Burrows & Hayes 1996; Müller et al. 2004; Kotake et al. 2006). In addition, the precollapse density inhomogeneities (e.g., Burrows & Hayes 1996; Müller & Janka 1997; Fryer 2004), nonaxisymmetric rotational instabilities (e.g., Rappaport et al. 1998; Ott et al. 2007),  $g$ -mode (e.g., Ott et al. 2006), and  $r$ -mode pulsations of PNSs (e.g., Andersson et al. 2011), and aspherical mass ejection may contribute to the overall GW signature.

In the later BH formation phase, the typical frequency of GW signals is relatively high (e.g., Pan et al. 2018). GW emission at BH formation in the collapsar scenario has been studied by some previous works (e.g., Sekiguchi & Shibata 2005; Ott et al. 2011; Cerdá-Durán et al. 2013; Pan et al. 2018). These works showed that the peak frequency from  $g$ -mode PNS oscillations at BH formation is expected to be above 2 kHz. However, such GW signals are very close to the limit of the current GW detectors and are difficult to detect. Overall, according to the GW emission mechanisms and current GW detectors, the most promising detectable frequency is at 100–1000 Hz in the collapsar phase. For a rotational core-collapse event, the average maximum amplitude of GWs at the distance  $R$  is calculated as (Dimmelmeier et al. 2002; Moore et al. 2015)

$$h_{\max} = 8.9 \times 10^{-21} \left( \frac{10 \text{ kpc}}{R} \right). \quad (13)$$

As shown in Figure 4, the GW signals from collapsars are likely to be detected by aLIGO and ET.

In the central engine phase (hyperaccretion phase), GWs are expected to be from the BH–inner-disk precession system (e.g., Sun et al. 2012) and the anisotropic neutrino emission from NDAFs (e.g., Suwa & Murase 2009; Liu et al. 2017a). In Sun et al. (2012), they studied the GWs of the jet precession based on NDAFs around spinning BHs. They argued that disk-driven jet precession may be common in a BH accretion system since the only necessary condition is that the angular momentum of the initial accretion flow is misaligned with the BH spinning axis. The GW signals from such systems are expected to be detectable at the frequency of tens of hertz and have comparable amplitudes to GW signals from the anisotropic neutrino emission. For GWs from the anisotropic neutrino emission, the detectable frequency is at 1–100 Hz, as shown in Figure 2. As discussed in Section 2.3, the progenitor mass and metallicity have little influence on GW signals. The maximum amplitude of GWs from NDAFs is roughly  $h_{\max} = 5 \times 10^{-22}$ .

In the GRB jet phase, the relativistic jets are expected to be GW sources and have been studied by some previous works (see, e.g., Segalis & Ori 2001; Sago et al. 2004; Akiba et al. 2013; Birnholtz & Piran 2013). Sago et al. (2004) analyzed the GWs from the accelerating phase of GRB jets based on the internal shock model. The ultrarelativistic nonspherically symmetrical acceleration of energetic jets is expected to emit GWs. For such GW signals, the maximum amplitude is  $\sim 10^{-22}$  at the frequency of  $\sim 0.1$  Hz at 10 kpc. Meanwhile, GW emission is also expected to be produced in the decelerating phase of GRB jets (e.g., Akiba et al. 2013). The GW amplitude is approximately  $\sim 10^{-24}$  Hz at the frequency of 10–100 Hz, which is too low to be detected. Therefore, in such a phase, the GW signals are more likely to be detected at 0.1–10 Hz by *DECIGO*/BBO and ultimate-*DECIGO*.

As the above discussion indicates, the GW signals related to the various mechanisms from the three phases have different characteristic frequencies. The collapsar phase occurs earlier than the central engine phase and GRB jet phase. From the perspective of detection, one would receive the high-frequency GW signals from collapsars first and then the low-frequency GW signals from later phases.

#### 4. Summary

In this work, we employed the pre-SN model and studied the GWs generated by the anisotropic neutrino emission from NDAFs in the center of collapsars. We found that the progenitor mass and metallicity have little influence on the GW emission. The GW signals from NDAFs in the center of the massive progenitor stars are more likely to be detected by GW detectors at a distance of 10 kpc. Then, we briefly summarized the GW emission in the different phases of collapsars. The primary detectable frequencies and strains in the three phases (the collapsar, central engine, and GRB jet phases) are different. Considering that the three phases occur in a time sequence, one may distinguish the detectable GWs from the different phases, which can partly verify the collapsar model and BH hyperaccretion solution.

Furthermore, it is inadequate to constrain the nature of the progenitors solely according to the GW detection. By combining the electromagnetic counterparts, neutrinos, and GWs, we might obtain the accurate and authentic properties of the progenitor stars and central BH accretion systems. In Song & Liu (2019), they constrained the characteristics of the progenitor stars of the GRB-SN case by LGRB-SN data. In Paper I, we have investigated the effects of the mass and metallicity of progenitor stars on the time-integrated spectrum of electron neutrinos from NDAFs. The detection of sub-MeV neutrinos may help us limit the metallicities of the progenitor stars.

We appreciate the assistance of Professor A. Heger who provided the pre-SN data. This work was supported by the National Natural Science Foundation of China under grant 11822304 and the Fundamental Research Funds for the Central Universities at Xiamen University under grant 20720190115.

#### ORCID iDs

Tong Liu  <https://orcid.org/0000-0001-8678-6291>

#### References

Abbott, B. P., Abbott, R., Abbott, T. D., et al. 2016, *PhRvL*, 116, 061102  
Abbott, B. P., Abbott, R., Abbott, T. D., et al. 2017, *PhRvL*, 119, 161101

Akiba, S., Nakada, M., Yamaguchi, C., et al. 2013, *PASJ*, 65, 59  
Andersson, N., Ferrari, V., Jones, D. I., et al. 2011, *GRGr*, 43, 409  
Barkov, M. V., & Komissarov, S. S. 2008, *MNRAS*, 385, L28  
Birnholtz, O., & Piran, T. 2013, *PhRvD*, 87, 123007  
Blandford, R. D., & Znajek, R. L. 1977, *MNRAS*, 179, 433  
Blondin, J. M., & Mezzacappa, A. 2006, *ApJ*, 642, 401  
Blondin, J. M., Mezzacappa, A., & DeMarino, C. 2003, *ApJ*, 584, 971  
Buras, R., Janka, H.-T., Rampp, M., et al. 2006, *A&A*, 457, 281  
Burrows, A., & Hayes, J. 1996, *PhRvL*, 76, 352  
Burrows, A., & Lattimer, J. M. 1983, *ApJ*, 270, 735  
Burrows, A., Livne, E., Dessart, L., et al. 2006, *ApJ*, 640, 878  
Burrows, A., Livne, E., Dessart, L., et al. 2007, *ApJ*, 655, 1416  
Cerdá-Durán, P., DeBrye, N., Aloy, M. A., et al. 2013, *ApJL*, 779, L18  
Chen, W.-X., & Beloborodov, A. M. 2007, *ApJ*, 657, 383  
Cutler, C., & Thorne, K. S. 2002, in Proc. of the 16th Int. Conf. on General Relativity and Gravitation, ed. N. Bishop & S. D. Maharaj (Singapore: World Scientific), 72  
Dimmelmeier, H., Font, J. A., & Müller, E. 2002, *A&A*, 393, 523  
Epstein, R. 1978, *ApJ*, 223, 1037  
Flanagan, É. É., & Hughes, S. A. 1998, *PhRvD*, 57, 4535  
Foglizzo, T., Galletti, P., Scheck, L., et al. 2007, *ApJ*, 654, 1006  
Fruchter, A. S., Levan, A. J., Strolger, L., et al. 2006, *Natur*, 441, 463  
Fryer, C. L. 2004, *ApJL*, 601, L175  
Fryer, C. L., & Heger, A. 2000, *ApJ*, 541, 1033  
Fryer, C. L., Holz, D. E., & Hughes, S. A. 2002, *ApJ*, 565, 430  
Fryer, C. L., Holz, D. E., & Hughes, S. A. 2004a, *ApJ*, 609, 288  
Fryer, C. L., Holz, D. E., Hughes, S. A., et al. 2004b, in Stellar Collapse, ed. C. L. Fryer (Dordrecht: Springer), 373  
Fryer, C. L., & New, K. C. B. 2011, *LRR*, 14, 1  
Galama, T. J., Vreeswijk, P. M., van Paradijs, J., et al. 1998, *Natur*, 395, 670  
Gu, W.-M., Liu, T., & Lu, J.-F. 2006, *ApJL*, 643, L87  
Heger, A., & Woosley, S. E. 2010, *ApJ*, 724, 341  
Herant, M. 1995, *PhR*, 256, 117  
Hjorth, J., Sollerman, J., Møller, P., et al. 2003, *Natur*, 423, 847  
Janiuk, A., & Proga, D. 2008, *ApJ*, 675, 519  
Janiuk, A., Yuan, Y., Perna, R., et al. 2007, *ApJ*, 664, 1011  
Janka, H.-T., Langanke, K., Marek, A., et al. 2007, *PhR*, 442, 38  
Janka, H.-T., & Müller, E. 1996, *A&A*, 306, 167  
Kashiyama, K., Nakauchi, D., Suwa, Y., et al. 2013, *ApJ*, 770, 8  
Kawanaka, N., & Mineshige, S. 2007, *ApJ*, 662, 1156  
Kohri, K., & Mineshige, S. 2002, *ApJ*, 577, 311  
Kotake, K. 2013, *CRPhy*, 14, 318  
Kotake, K., Ohnishi, N., & Yamada, S. 2007, *ApJ*, 655, 406  
Kotake, K., Sato, K., & Takahashi, K. 2006, *RPPH*, 69, 971  
Kotake, K., Takiwaki, T., & Harikae, S. 2012, *ApJ*, 755, 84  
Kumar, P., & Zhang, B. 2015, *PhR*, 561, 1  
Lee, H. K., Brown, G. E., & Wijers, R. A. M. J. 2000a, *ApJ*, 536, 416  
Lee, H. K., Wijers, R. A. M. J., & Brown, G. E. 2000b, *PhR*, 325, 83  
Lee, W. H., Ramirez-Ruiz, E., & Page, D. 2005, *ApJ*, 632, 421  
Lei, W. H., Wang, D. X., Zhang, L., et al. 2009, *ApJ*, 700, 1970  
Lei, W.-H., Zhang, B., & Liang, E.-W. 2013, *ApJ*, 765, 125  
Lei, W.-H., Zhang, B., Wu, X.-F., et al. 2017, *ApJ*, 849, 47  
Liu, T., Gu, W.-M., Xue, L., et al. 2007, *ApJ*, 661, 1025  
Liu, T., Gu, W.-M., & Zhang, B. 2017a, *NewAR*, 79, 1  
Liu, T., Lin, C.-Y., Song, C.-Y., et al. 2017b, *ApJ*, 850, 30  
Liu, T., Lin, Y.-Q., Hou, S.-J., et al. 2015, *ApJ*, 806, 58  
Liu, T., Song, C.-Y., Yi, T., et al. 2019, *JHEAp*, 22, 5  
Liu, T., Song, C.-Y., Zhang, B., et al. 2018, *ApJ*, 852, 20  
Liu, T., Zhang, B., Li, Y., et al. 2016, *PhRvD*, 93, 123004  
MacFadyen, A. I., & Woosley, S. E. 1999, *ApJ*, 524, 262  
Malesani, D., Tagliaferri, G., Chincarini, G., et al. 2004, *ApJL*, 609, L5  
Marek, A., Janka, H.-T., & Müller, E. 2009, *A&A*, 496, 475  
Matsumoto, T., Nakauchi, D., Ioka, K., et al. 2015, *ApJ*, 810, 64  
Maurer, J. I., Mazzali, P. A., Deng, J., et al. 2010, *MNRAS*, 402, 161  
McKinney, J. C., & Gammie, C. F. 2004, *ApJ*, 611, 977  
Mizuno, Y., Yamada, S., Koide, S., et al. 2004, *ApJ*, 615, 389  
Modjaz, M., Stanek, K. Z., Garnavich, P. M., et al. 2006, *ApJL*, 645, L21  
Moenchmeyer, R., Schaefer, G., Müller, E., et al. 1991, *A&A*, 246, 417  
Moore, C. J., Cole, R. H., & Berry, C. P. L. 2015, *CQGra*, 32, 015014  
Müller, E. 1982, *A&A*, 114, 53  
Müller, E., & Janka, H.-T. 1997, *A&A*, 317, 140  
Müller, E., Rampp, M., Buras, R., et al. 2004, *ApJ*, 603, 221  
Nagataki, S. 2009, *ApJ*, 704, 937  
Nagataki, S. 2018, *RPPH*, 81, 026901  
Nakauchi, D., Kashiyama, K., Suwa, Y., et al. 2013, *ApJ*, 778, 67  
Narayan, R., Piran, T., & Kumar, P. 2001, *ApJ*, 557, 949

- O'Dea, C. P. 2002, [NewAR](#), **46**, 41
- Ott, C. D. 2009, [CQGra](#), **26**, 063001
- Ott, C. D., Burrows, A., Dessart, L., et al. 2006, [PhRvL](#), **96**, 201102
- Ott, C. D., Burrows, A., Dessart, L., et al. 2008, [ApJ](#), **685**, 1069
- Ott, C. D., Burrows, A., Livne, E., et al. 2004, [ApJ](#), **600**, 834
- Ott, C. D., Dimmelmeier, H., Marek, A., et al. 2007, [PhRvL](#), **98**, 261101
- Ott, C. D., Reisswig, C., Schnetter, E., et al. 2011, [PhRvL](#), **106**, 161103
- Pan, K.-C., Liebendörfer, M., Couch, S. M., et al. 2018, [ApJ](#), **857**, 13
- Pian, E., Mazzali, P. A., Masetti, N., et al. 2006, [Natur](#), **442**, 1011
- Popham, R., Woosley, S. E., & Fryer, C. 1999, [ApJ](#), **518**, 356
- Rampp, M., Mueller, E., & Ruffert, M. 1998, [A&A](#), **332**, 969
- Sago, N., Ioka, K., Nakamura, T., et al. 2004, [PhRvD](#), **70**, 104012
- Scheck, L., Janka, H.-T., Foglizzo, T., et al. 2008, [A&A](#), **477**, 931
- Segalis, E. B., & Ori, A. 2001, [PhRvD](#), **64**, 064018
- Sekiguchi, Y.-I., & Shibata, M. 2005, [PhRvD](#), **71**, 084013
- Song, C.-Y., & Liu, T. 2019, [ApJ](#), **871**, 117
- Song, C.-Y., Liu, T., Gu, W.-M., et al. 2016, [MNRAS](#), **458**, 1921
- Stanek, K. Z., Matheson, T., Garnavich, P. M., et al. 2003, [ApJL](#), **591**, L17
- Sun, M.-Y., Liu, T., Gu, W.-M., et al. 2012, [ApJ](#), **752**, 31
- Suwa, Y., & Ioka, K. 2011, [ApJ](#), **726**, 107
- Suwa, Y., & Murase, K. 2009, [PhRvD](#), **80**, 123008
- van Putten, M. H. P. M. 2001, [PhR](#), **345**, 1
- van Putten, M. H. P. M., Della Valle, M., & Levinson, A. 2011, [A&A](#), **535**, L6
- van Putten, M. H. P. M., Della Valle, M., & Levinson, A. 2019, [ApJL](#), **876**, L2
- van Putten, M. H. P. M., & Levinson, A. 2003, [ApJ](#), **584**, 937
- van Putten, M. H. P. M., Levinson, A., Frontera, F., et al. 2019, [EPJP](#), **134**, 537
- van Putten, M. H. P. M., & Ostriker, E. C. 2001, [ApJL](#), **552**, L31
- Wei, Y.-F., Liu, T., & Song, C.-Y. 2019, [ApJ](#), **878**, 142
- Woosley, S. E. 1993, [ApJ](#), **405**, 273
- Woosley, S. E., & Bloom, J. S. 2006, [ARA&A](#), **44**, 507
- Woosley, S. E., & Heger, A. 2007, [PhR](#), **442**, 269
- Woosley, S. E., & Heger, A. 2012, [ApJ](#), **752**, 32
- Woosley, S. E., Heger, A., & Weaver, T. A. 2002, [RvMP](#), **74**, 1015
- Wu, X.-F., Hou, S.-J., & Lei, W.-H. 2013, [ApJL](#), **767**, L36
- Xue, L., Liu, T., Gu, W.-M., et al. 2013, [ApJS](#), **207**, 23
- Yamada, S., & Sato, K. 1995, [ApJ](#), **450**, 245
- Zalamea, I., & Beloborodov, A. M. 2011, [MNRAS](#), **410**, 2302
- Zhang, B. 2018, *The Physics of Gamma-Ray Bursts* (Cambridge: Cambridge Univ. Press)
- Zhang, W., Woosley, S. E., & Heger, A. 2004, [ApJ](#), **608**, 365
- Zwerg, T., & Müller, E. 1997, [A&A](#), **320**, 209